The Role for an Invariant Aspartic Acid in Hypoxanthine Phosphoribosyltransferases Is Examined Using Saturation Mutagenesis, Functional Analysis, and X-ray Crystallography†

Bhutorn Canyuk,‡,§ Pamela J. Focia,‡,# and Ann E. Eakin*,‡,||

Laboratory of Molecular Parasitology & Drug Design, Division of Medicinal Chemistry and Natural Products, School of Pharmacy, and Department of Biochemistry and Biophysics, School of Medicine, University of North Carolina, Chapel Hill, North Carolina 27599-7360

Received May 25, 2000; Revised Manuscript Received January 9, 2001

ABSTRACT: The role of an invariant aspartic acid (Asp137) in hypoxanthine phosphoribosyltransferases (HPRTs) was examined by site-directed and saturation mutagenesis, functional analysis, and X-ray crystallography using the HPRT from *Trypanosoma cruzi*. Alanine substitution (D137A) resulted in a 30-fold decrease of k_{cat}, suggesting that Asp137 participates in catalysis. Saturation mutagenesis was used to generate a library of mutant HPRTs with random substitutions at position 137, and active enzymes were identified by complementation of a bacterial purine auxotroph. Functional analyses of the mutants, including determination of steady-state kinetic parameters and pH-rate dependence, indicate that glutamic acid or glutamine can replace the wild-type aspartate. However, the catalytic efficiency and pH−rate profile for the structural isosteric mutant, D137N, were similar to the D137A mutant. Crystal structures of four of the mutant enzymes were determined in ternary complex with substrate ligands. Structures of the D137E and D137Q mutants reveal potential hydrogen bonds, utilizing several bound water molecules in addition to protein atoms, that position these side chains within hydrogen bond distance of the bound purine analogue, similar in position to the aspartate in the wild-type structure. The crystal structure of the D137N mutant demonstrates that the Asn137 side chain does not form interactions with the purine substrate but instead forms novel interactions that cause the side chain to adopt a nonfunctional rotamer. The results from these structural and functional analyses demonstrate that HPRTs do not require a general base at position 137 for catalysis. Instead, hydrogen bonding sufficiently stabilizes the developing partial positive charge at the N7-atom of the purine substrate in the transition-state to promote catalysis.

Hypoxanthine phosphoribosyltransferase (HPRT,[1] EC 2.4.2.8.) is a key enzyme in the salvage pathway for the synthesis of purine nucleotides. HPRT catalyzes the transfer of a phosphoribosyl group from 5-phospho-α-D-ribosyl-1-pyrophosphate (PRPP) to a 6-oxopurine base (either hypoxanthine or guanine, and in some species xanthine) to form pyrophosphate (PPi) and the corresponding purine nucleotide [either inosine monophosphate (IMP), guanosine monophosphate (GMP), or xanthosine monophosphate (XMP)] (Scheme 1). HPRT has been proposed as a potential target for the chemotherapeutic treatment of various parasitic infections (*1*−*3*), and recently, inhibitors of the HPRT from *Trypanosoma cruzi*, etiologic agent of Chagas' disease, were shown to slow the growth of parasites in mammalian cells in culture (*4*). Deficiency of HPRT activity in humans is caused by several inherited mutations and can result in severe metabolic diseases, such as Lesch−Nyhan syndrome or gouty arthritis (*5*). In recent years, a number of crystal structures of HPRTs from human and various pathogenic parasites have been determined with different ligands bound (*6*−*15*). These structures provide insight into the potential roles of conserved and invariant amino acids that may participate in HPRT function (*16*).

† This work was supported by National Institutes of Health Grants AI38919 and AI45021 (to A.E.E.) and a graduate fellowship from the Royal Thai Government (to B.C.). The Stanford Synchrotron Radiation Laboratory Biotechnology Program is supported by the National Institutes of Health, National Center for Research Resources, Biomedical Technology Program and the Department of Energy, Office of Biological and Environmental Research. The Advanced Photon Source (APS), at Argonne National Laboratory, is supported by the U.S. National Science Foundation through Grant DMR-9304725 and the State of Illinois through the Department of Commerce and the Board of Higher Education Grant IBHE HECA NWU 96, and the U.S. Department of Energy, Basic Energy Sciences, Office of Energy Research under Contract No. W-31-102-Eng-38. One dataset was measured during the Datacol '99 course held at the National Synchrotron Light Source, Brookhaven National Laboratory, which is supported by the U.S. Department of Energy, Division of Chemical Science under Contract No. DE-AC02-98CH10886.

* To whom correspondence should be addressed. E-mail: eakin@unc.edu. Phone: (919) 966-6422. Fax: (919) 966-0204.

‡ School of Pharmacy.

|| School of Medicine.

§ Current address: Prince of Songkla University, Department of Pharmaceutical Chemistry, Hat-Yai, Songkla 90112, Thailand.

Current address: Northwestern University Molecular Pharmacology and Biological Chemistry, Chicago, IL 60611.

[1] Abbreviations: GMP, guanosine monophosphate; HPP, 7-hydroxy-[4,3-*d*]pyrazolopyrimidine; HPRT, hypoxanthine phosphoribosyltransferase; IMP, inosine monophosphate; PEG, poly(ethylene glycol); PPi, pyrophosphate; PRPP, 5-phospho-α-D-ribosyl-1-pyrophosphate; WT, wild-type; XMP, xanthosine monophosphate; XPRT, xanthine phosphoribosyltransferase.

10.1021/bi001195q CCC: $20.00
Published on Web 02/07/2001

Scheme 1. The HPRT-Catalyzed Reaction

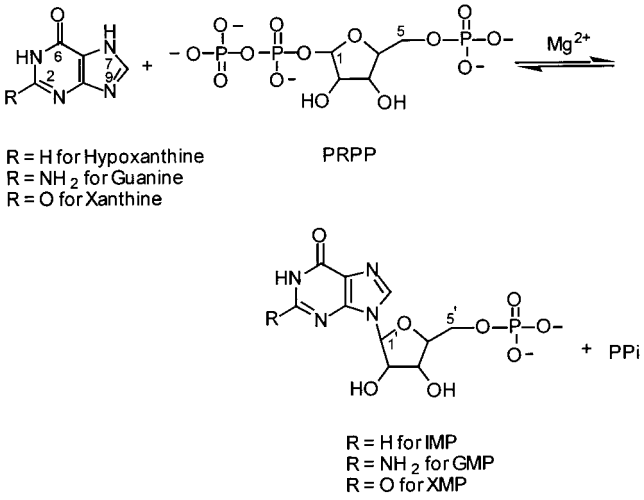

Aspartic acid at position 137 (Asp137, according to the numbering for the human enzyme) is an invariant residue among 6-oxopurine phosphoribosyltransferases, including HPRTs and XPRTs. The position of Asp137 in the active sites of these enzymes, as shown by their crystal structures, suggests that the acidic side chain performs a common function in the enzyme-catalyzed reactions (*6*−*17*). Asp137 was originally proposed to function as a general base to deprotonate purine substrates via N7 in the forward reaction, based on the human crystal structure with bound product, GMP (*6*). Xu and Grubmeyer (*18*) further concluded that Asp137 functions as a general base based on biochemical analysis of the wild-type and D137N mutant of the human HPRT.

In the present study, we examine the potential role of Asp137 by both functional and structural analyses of various mutants at position 137. The functional contribution of the carboxylate side chain of Asp137 was initially assessed by site-specific alanine substitution. Kinetic analysis of the D137A mutant suggests that the carboxylate side chain of Asp137 participates in the chemical step of catalysis. To provide further insight into the chemical requirements for the side chain at position 137, we used saturation site-directed mutagenesis to create multiple substitutions at position 137 (*19*, *20*). Saturation mutagenesis generates a library of mutant enzymes in which the target residue is replaced by each of the 20 amino acids plus a stop codon. Furthermore, a functional assay was devised to rapidly select for catalytically active HPRTs from the random library using complementation of a bacterial purine auxotroph (*21*). Steady-state kinetics parameters and pH−rate dependence were determined for selected mutants to assess the effects of the substitutions on enzyme function.

Crystal structures of four of these mutants were determined to investigate in detail the structural consequences caused by substitutions at residue 137. For these structures, the enzymes were crystallized in ternary substrates complex with a purine analogue, 7-hydroxy[4,3-*d*]pyrazolopyrimidine (HPP), and magnesium-complexed PRPP, similar to a previous structure of the WT trypanosomal HPRT (*11*). This strategy results in a crystal form that yields structures of the functional dimer with two independent views of substrates bound HPRT active site. In one subunit, a flexible loop (loop II) is in an open conformation with bound ligands accessible to bulk solvent, providing an approximate view of the active site during substrate binding. In the other subunit of the dimer, loop II is in a closed conformation creating a fully formed active site in which the bound ligands are secluded from the aqueous milieu. This closed conformation of the active site approximates the catalytically competent enzyme−substrates complex just prior to catalysis. The structures of the mutants at position 137 support the functional assays and help to clarify the effects of the mutations on HPRT activity. The results reported here indicate that HPRTs do not require a general base at position 137 for catalysis, but instead hydrogen bonding with the N7 of the purine base is sufficient for stabilization of the transition state.

MATERIALS AND METHODS

Materials. Restriction enzymes and T4 DNA ligase were purchased from New England Biolabs (Beverly, MA) and Boehringer Mannheim (Indianapolis, IN). Δ*Taq* DNA polymerase and nucleotides were purchased from United States Biochemicals (Cleveland, OH). Sequenase DNA Sequencing kits and Thermo Sequenase radiolabeled terminator cycle sequencing kits were obtained from Amersham Life Science (Arlington Heights, IL). Oligonucleotide primers were synthesized by Gibco BRL Life Technologies (Gaithersberg, MD). [α-^{35}S]dATP and [8-^{14}C]hypoxanthine were purchased from Dupont Merck Pharmaceutical Co. (Boston, MA). All other common chemicals and reagents, including GMP on 4% beaded agarose, were obtained from Sigma (St. Louis, MO).

Bacterial Strains and Plasmids. *Escherichia coli* strain DH5α competent cells were purchased from Gibco BRL Life Technologies (Gaithersburg, MD). The *rec A* strain of *E. coli* SØ606 (*ara*, Δ*pro-gpt-lac*, *thi*, *hpt*, *recA*) (*22*) was provided by Duncan Cochran (University of Queensland, Australia). *E. coli* strain SØ609 (*ara*, Δ*pro-gpt-lac*, *thi*, *hpt*, *pup*, *pur H*, *J*, *strA*) (*22*) was provided by Per Nygaard (University of Copenhagen, Denmark). The pBAce expression plasmid (*23*) was used to produce HPRT in *E. coli* strains as previously described (*24*).

Specific Site-Directed Mutagenesis. Alanine substitution at Asp137 (D137A) was performed by the PCR overlap extension method (*25*). The sequence of the four oligonucleotide primers were primer 1 (5′-flanking, sense sequence) 5′-TGTGGTGGCCTCGAAATTCTGTCA-3′; primer 2 (overlap, sense sequence) 5′-GGATATCGTTGCCACCGCCCTCAC-3′; primer 3 (overlap, antisense sequence) 5′-GTGGCAACGATATCCTCCACAATCAAC-3′; primer 4 (3′-flanking, antisense sequence) 5′-GTTTTCCCAGTCACGACGTTGA-3′. The underlined letters include mismatches for the introduction of silent mutation to create an *EcoRV* recognition site (GATATC), as well as the alanine substitution (GCC). The *EcoRV* recognition site was introduced to facilitate the construction of the saturation mutagenesis plasmids (described below). The 336-bp PCR-amplified mutagenic cassette was purified and subcloned into the HPRT expression plasmid (*24*) to replace the WT sequence. Plasmids were sequenced by the dideoxy chain termination method to confirm the mutations and verify the entire sequence of the PCR-amplified region.

Saturation Site-Directed Mutagenesis. The primers used for the construction of saturation mutagenic fragments by PCR were primer 5 (5′-flanking, sense sequence) 5′-

GGAGGATATCGTTNNSACCGCCCTCACGC-3′ and primer 4 (3′-flanking, antisense sequence, as above). Fragments with the random mixture of codons were PCR-amplified, purified, digested with *EcoRV* and *PstI* and subcloned into similarly prepared D137A expression plasmids. The ligation mixtures were transformed into MAX-efficiency DH5α competent cells and plated on nutrient (NZCYM) (*26*) agar containing ampicillin (100 μg/mL), adenine (15 μg/mL), and guanosine (30 μg/mL) (*21*). The plasmid library encoding mutant HPRTs was obtained by flooding the colonies on the plate with liquid NZCYM containing ampicillin (100 μg/mL), adenine (15 μg/mL), and guanosine (30 μg/mL). This media was collected and cultured to amplify the pool of plasmids under nonselective conditions, and the plasmid library was purified from the cells by standard techniques (*26*).

Functional Complementation Screening. The plasmid library was transformed into *E. coli* strain SØ609 (*22*) using the $CaCl_2$ method (*26*). Three equal aliquots of the transformed cells were then plated on three different solid media systems: (i) nutrient (NZCYM) agar supplemented with adenine (15 μg/mL) and guanosine (30 μg/mL) as a nonselective control, (ii) low phosphate semidefined media (*21*) agar supplemented with hypoxanthine (73 μM) and guanine (66 μM), or (iii) low phosphate semidefined media agar supplemented with guanine (132 μM). The plates, which also contained ampicillin (100 μg/mL) and streptomycin (25 μg/mL), were incubated at 37 °C for 16 h.

DNA Sequencing. Plasmids were sequenced directly from bacterial colonies using a modified method of that described previously (*27*, *28*). Single colonies were selected from the functional assay plates, streaked on nonselective media (NZCYM) agar, and grown for 16 h at 37 °C to amplify the bacteria. The amplified colonies were resuspended in 12 μL of TE buffer (10 mM Tris-HCl, pH 8.0, 1 mM EDTA, pH 8.0) containing Proteinase K (50 μg/mL). The suspension was incubated at 55 °C for 15 min followed by 80 °C for 15 min. The samples were chilled on ice before microcentrifuging for 5 min. The supernatants (7 μL) were collected and used directly as templates for DNA sequencing using the [α-^{33}P]-labeled ddNTP terminator kit from Amersham (Arlington Heights, IL).

Characterization of the Functional Screening System. To characterize the stringency of the functional selection assay, plasmids with DNA encoding WT and mutant HPRTs (D137E, D137Q, D137N, D137C, D137A, D137V, and D137L) were individually transformed into *E. coli* SØ609 and plated on the three media systems described above. The plates were incubated at 37 °C, and the growth of each transformant was visually assessed for a 90-h period, to correlate HPRT activity with the growth rate of complemented SØ609 bacteria.

Expression and Purification of Recombinant Wild-Type and Mutant HPRTs. For recombinant protein production, expression plasmids were transformed into *E. coli* SØ606 (*22*). The transformants were cultured in low-phosphate induction media with modifications (15 μg/mL of adenine and 30 μg/mL of guanosine instead of 20 μg/mL of adenine and guanine), and recombinant enzymes were purified by affinity chromatography using GMP-agarose as previously described (*24*). GMP was removed from the purified mutant HPRTs by size-exclusion chromatography using a fast desalting column (Pharmacia Biotech). Elution of the recombinant HPRT in Bis−Tris−Mg buffer (20 mM Bis-Tris, pH 7.0, 6 mM $MgCl_2$) was monitored by absorption at 280 nm. For crystallization, the purified HPRT was concentrated using a Centriprep-10 concentrator (Amicon, Beverly, MA). Enzyme concentrations were determined by the Bradford method using IgG as the protein standard (Protein Assay kit, Bio-Rad, Hercules, CA).

Enzyme Assays. Specific activities for the forward reaction (IMP synthesis) were determined by radiochemical assay using ^{14}C-hypoxanthine (20 μM), unlabeled hypoxanthine (80 μM), and PRPP (1 mM) as previously described (*24*, *29*, *30*). Kinetic parameters for the forward reaction were determined using a spectrophotometric method previously described (*30*, *31*). All measurements were carried out in 100 mM Tris-HCl, pH 7.5, and 12 mM $MgCl_2$ at 37 °C. Initial velocities were determined at varying substrate concentrations in the presence of excess fixed substrate (5 × K_m). The K_m and k_{cat} values were determined by nonlinear regression analysis using the kcat software, version 1.5 (BioMetallic, Inc, Princeton, NJ).

The pH−Activity Relationships. The initial velocities for the forward reaction at various pH values were measured using the spectrophotometric method (*30*, *31*) at 400 μM PRPP and hypoxanthine at three different concentrations (100, 300, and 400 μM) to confirm that saturating conditions for hypoxanthine had been achieved. The velocity measurements were constant for the WT, D137E, D137N, and D137A mutants at the various buffer conditions for each hypoxanthine concentration, and thus the values plotted at 400 μM hypoxanthine yield apparent k_{cat}'s for the plots. At pH values above 7.0, the velocities for the D137Q mutant increased with increasing hypoxanthine, indicating that the substrate was no longer saturating even at 400 μM. However, the limit of solubility for hypoxanthine in the assays was 400 μM; thus, the rates presented for D137Q at pH values above 7.0 are no longer reflective of k_{cat}. The rates plotted for the D137G and D137V mutants were determined at 200 μM hypoxanthine. Buffers (at 100 mM) were chosen to test the following pH ranges: acetate, pH 4−5; MOPS, pH 6−8; MES, pH 6.1−7.1; Tris, pH 7−9; CHES, pH 8.3−9.3; and CAPSO, pH 9.6. Sodium chloride was added to the reaction solutions to maintain constant ionic strength at 0.112 M.

Crystallization. Hanging drop vapor diffusion was employed in the cocrystallization of recombinant HPRTs with substrate ligands (PRPP and HPP). Each protein−ligand solution contained purified mutant HPRT in Bis−Tris−Mg buffer (20 mM Bis−Tris, pH 7.0, 6 mM $MgCl_2$), 10 mM PRPP, and 10 mM HPP. Stock solutions (100 mM) of the ligands were first prepared with PRPP in Bis-Tris-Mg buffer and the HPP in DMSO. These stock solutions were added to the protein/buffer solution in the predicted order of substrate binding; thus, the PRPP stock solution (1/10 volume) was incubated with the enzyme briefly before adding the HPP stock solution (1/10 volume). The precipitant solutions were composed of 15−20% PEG 6000, 0.1 M sodium acetate buffer (pH 4.4−5.0), and 0.2 M ammonium acetate. Each hanging drop was composed of 2 μL of protein−ligand solution plus 2 μL of precipitant solution. Trays were incubated at 4 °C and monoclinic crystals formed within one week. Although ternary complex crystals for each of the mutants appeared over a small range of pH, protein,

and PEG concentrations, those used for the determination of the crystal structures are specified below. The stated pHs result from a 1:1 ratio of protein−ligand solution to precipitating solution. The pH, protein, and PEG concentrations for the mutant crystal structures were D137A (4.6, 6 μg/μL, and 20%), D137N (5.0, 6 μg/μL, and 15.5%), D137Q (5.0, 6 μg/μL, and 17%), and D137E (5.0, 7 μg/μL, and 18.5%).

Measurement and Processing of Diffraction Data. Single crystals were transferred to cryoprotectant solutions, which were prepared by addition of 15% PEG 400 to the precipitating solution from which the crystals were grown. The crystals were mounted in nylon loops and either placed directly into the cryostream, or flash-cooled and stored in liquid nitrogen prior to data collection. All datasets were measured in a single sweep of between 120 and 200 degrees with oscillation angles of between 0.75 and 1.5 degrees, depending on the circumstances of each experiment. Diffraction data were processed with the HKL package (*32*). Several percent of the structure factors from each dataset (5−8%) were set aside for calculation of free R-factors (*33*). Since only minor variations in the unit cell dimensions were observed among the four mutant datasets and that for the original wild-type structure (*11*), we approached all structure determinations in the same way, using as the initial phasing model, a modified wild-type ternary complex dimer in which ligands, residue 137 and water molecules were deleted in each subunit. The protein model was placed into each dataset by sequential one and two rigid body refinement with increasing resolution limits (15 to 6 Å, 15 to 4.5 Å, 15 to 3.5 Å resolution) using XPLOR (*34*). This was followed by simulated annealing, positional and temperature factor refinement, incorporating data from 6 Å to an intermediate resolution limit for each individual dataset (generally between 2.2 and 2.0 Å). For each structure, the initial electron density maps ($2F_o - F_c$ and $F_o - F_c$) permitted positioning of the ligands (PRPP complexed with two hydrated magnesium ions and HPP) into each active site of the asymmetric dimer. The models were manually adjusted using the program O (*35*). Additional water molecules were added where $F_o - F_c$ electron density peaks greater than 3 standard deviations of the map were found and where at least one suitable hydrogen bond partner was present. Several additional rounds of positional and temperature factor refinement and inspection of electron density maps were adequate to make all necessary changes in each mutant model. The high resolution limit for each dataset was determined empirically by gradual addition of data to the refinements. Although the merging R-factors for data in the highest resolution bins were near 40% for the D137A, D137E, and D137Q mutants, the data were included in the refinement if doing so improved the free R-factor and the maps. Omit maps were used to verify the positions of the ligands, and residues and water molecules of interest in the final models. Figures 2, 3, and 5 were prepared with SETOR (*36*). The atomic coordinates and structure factors of the mutant enzymes have been deposited in the Protein Data Bank, with the following accession codes: 1I13 (D137A), 1I14 (D137E), 1I0L (D137N), and 1I0I (D137Q).

RESULTS AND DISCUSSION

Saturation Mutagenesis and Functional Selection in Bacteria. Alanine substitution at Asp137 (D137A) markedly decreased enzyme activity to only 1% that of WT activity, suggesting that the Asp137 carboxylate side chain participates in catalysis. To further examine the functional role of Asp137, the structural and functional consequences of replacing the aspartate side chain with other functional groups were evaluated to obtain a complete structure/function relationship for this invariant residue. To avoid the bias inherent in creating specific, selected mutations of the residue of interest, a more random approach using site-specific saturation mutagenesis (*19*, *20*) was used to generate a library of mutant HPRTs at position 137. Saturation mutagenesis was performed, according to a modified PCR-mutagenesis technique (*37*), using a mixture of mutagenic oligonucleotide primers. This primer mixture contained a 32-fold degenerate NNS sequence (where N = a mixture of A + C + G + T and S = a mixture of C + G), yielding codons for all 20 amino acids plus the amber stop codon at the mutagenic site. The PCR-amplified gene fragment was subsequently ligated back into the expression vector to create a library of plasmids encoding HPRT genes with random mutations at position 137.

Table 1: Sequences of Codons at Position 137 from Bacterial Colonies Identified in the Functional Selection Assay

codon[a]	NZCYM	H + G	G	codon	NZCYM	H + G	G
GCC (A)	1	0	0	CGC (R)	1	0	0
TGC (C)	1	0	0	AGC (S)	2	0	0
GAC (D)	1	8	3	TCC (S)	2	0	0
GAG (E)	1	6	1	TCG (S)	1	0	0
GGC (G)	2	0	0	ACC (T)	1	0	0
GGG (G)	4	0	0	ACG (T)	1	0	0
CTC (L)	1	0	0	GTC (V)	2	0	0
AAC (N)	1	0	0	TGG (W)	1	0	0
CAG (Q)	0	1	0	TAG (stop)	2	0	0
total	**12**	**15**	**4**	**total**	**13**	**0**	**0**

[a] The letters in the parentheses refer to the one letter symbols for the amino acids encoded by the corresponding genetic codons. NZCYM refers to nonselective nutrient media supplemented with adenine and guanosine. H + G or G refers to semidefined media supplemented with both hypoxanthine and guanine or only guanine, respectively. The numbers in the table represent the frequency of the identified codons from the direct sequencing of the bacterial clones.

A functional assay was introduced, using a bacterial purine auxotroph, for the selection of clones expressing catalytically active HPRTs. The SØ609 strain of *E. coli* is deficient in enzymes required for the de novo biosynthetic and salvage pathways for purine nucleotides (*22*), such that it requires complementation by a recombinant HPRT for growth on minimal media supplemented with hypoxanthine and/or guanine (*21*). SØ609 cells transformed with the library of plasmids obtained from saturation mutagenesis were plated on selective media systems containing either hypoxanthine and guanine, or guanine alone, as well as on nonselective nutrient media. The results of the functional selection of bacteria transformed with the Asp137 saturation library are shown in Table 1. Clones expressing D137E, D137Q, and WT enzymes were identified from sequencing 15 colonies from plates supplemented with hypoxanthine and guanine. Only WT and the D137E mutant were among the four clones that appeared on plates with guanine alone. To assess the diversity of codons at position 137 in the library, 25 clones of SØ609 bacteria transformed with the saturation plasmid library were picked from the nonselective media and sequenced, resulting in the identification of 17 different

Table 2: Correlation between Specific Activity for IMP Formation and Growth Rates on Nonselective and Selective Media of Bacteria Complemented by Wild-Type or Mutant HPRTs

	SA[a]	NZCYM	H + G			G		
		(17)[b]	(17)	(37)	(90)	(17)	(37)	(90)
WT	29 ± 1.7	++	++	++	++	++	++	++
D137E	18 ± 0.63	++	++	++	++	++	++	++
D137Q	6.2 ± 0.38	++	++	++	++	−	++	++
D137N	1.1 ± 0.05	++	−	++	++	−	−	+
D137C	1.1 ± 0.01	++	−	+	++	−	−	+
D137A	0.38 ± 0.01	++	−	−	++	−	−	+
D137V	0.19 ± 0.05	++	−	−	+	−	−	+
D137L	0.05 ± 0.00	++	−	−	+	−	−	+

[a] SA indicates specific activity expressed as μmol min^{-1} mg^{-1}. [b] The numbers in parentheses represent the incubation time (in hours) before bacterial colonies were visually assessed on the plates incubated at 37 °C. NZCYM refers to nonselective nutrient media supplemented with adenine and guanosine. H + G or G refers to semidefined media supplemented with hypoxanthine and guanine or guanine alone, respectively. The ++, +, or − classifies the bacterial growth as visible (small to large) colonies, extremely tiny colonies or no visible colonies, respectively.

codons encoding 12 amino acids and an amber codon (Table 1). Statistically, a truly random set of 32 codons would be predicted to yield 17.6 different codons from sequencing 25 clones (*38*). Although only 13 of the possible 20 amino acids were confirmed by random sequencing, these results indicate that the combinatorial library likely contained codons for all 20 amino acids.

The stringency of the bacterial functional assay system was assessed further by comparing the growth rates of the individual clones in SØ609 complemented by the WT and mutant HPRTs, with the relative specific activities of the purified enzymes, ranging from 60% (D137E) to 0.2% (D137L), as shown in Table 2. As a positive control, cells transformed with all mutants and WT plasmids exhibited comparable growth rates on nonselective nutrient media. In contrast, SØ609 bacteria complemented with the catalytically active mutant HPRTs grew at different rates on minimal media, and these rates correlate well with the activities of the purified enzymes (Table 2). Mutant HPRTs with 20−100% of the WT activity resulted in visible bacterial colonies after 17 h on selective media supplemented with hypoxanthine and guanine, and those with 0.6−4% activity required 37−90 h to yield visible colonies on this media. The growth rates also were consistent with the activities of purified enzymes when selective liquid media was used to quantitate growth rates by measuring optical density (results not shown). Guanine was far less efficient than hypoxanthine in supporting the growth of HPRT complemented SØ609 cells when it was the sole purine source in minimal media (*21*). Therefore, the media supplemented with guanine alone provides higher stringency for the selection of highly active mutant HPRTs than does the media containing both hypoxanthine and guanine (Table 2).

The *phoA* promoter in pBAce regulates the expression of recombinant enzyme that is required for the growth of SØ609 bacteria in selective media. This promoter is leaky (*39*), and during early stages of growth before depletion of phosphate in the media, the leaky expression is sufficient to initiate the growth of SØ609 complemented by mutant HPRTs with moderate to high activity. Expression of the recombinant HPRTs in SØ609 cells was monitored over time (10−45 h) by SDS−PAGE analysis and found to be consistent with the observed activities and relative growth rates for the mutants (data not shown). Bacterial complementation systems formerly used to select for active mutant enzymes have suffered from the disadvantage of using strong, inducible promoters to drive the overexpression of the recombinant enzyme (*19*, *20*). As a result, the high levels of the recombinant enzyme enabled mutants with very low activity to rescue the auxotrophic bacteria, resulting in a low stringency selection system. The *phoA* expression system involves complementation of SØ609 cells by recombinant enzyme produced at low levels by the leaky promotor in the presence of phosphate. Overexpression of HPRT does not occur until the phosphate has been depleted from the media (after >30 h growth at 37 °C). Thus, the bacterial complementation system described here provides a stringent functional assay with which preliminary structure−function relationships for specific side chains can be rapidly assessed by sequencing plasmids from a relatively modest number of colonies grown on selective media. Desired mutants with lower activities can then be recovered from nonselective media plates or created individually.

Overexpression and Purification of Recombinant Enzymes. Induction of the bacterial *phoA* promoter by growth of cultures for 36−48 h in conditions of phosphate starvation results in high yields of soluble, enzymatically active recombinant enzymes in SØ606 bacteria (*23*). For these studies, recombinant HPRTs were purified to near homogeneity by affinity chromatography using GMP-agarose (*24*). All of the various mutant enzymes bound to the GMP column, indicating that the mutations did not cause serious structural perturbations in the enzymes. These methods provided large quantities of purified enzymes for both kinetic analysis and structure determination.

Steady-State Kinetic Studies. Steady-state kinetic parameters for the WT and several mutant HPRTs are shown in Table 3. The growth rates of complemented SØ609 bacteria (Table 2) correlate well with the k_{cat} values of mutant enzymes (Table 3), demonstrating that the functional assay provides a useful tool for rapidly assessing the activities of mutants in structure−function studies of amino acid residues in the HPRT-catalyzed reaction. Comparison of the kinetic parameters for the mutant and WT HPRTS provides an indication of the functional consequence of the side chain substitution on substrate binding (reflected by the apparent K_m), on catalysis and product release (reflected by k_{cat}) and on overall catalytic efficiency (k_{cat}/K_m). Pre-steady-state kinetics and ligand binding analyses of the human HPRT demonstrated that the rate-limiting step for the enzyme-catalyzed reaction was product release (*9*, *18*). Thus, although similar detailed kinetic studies have not been completed for other HPRTs, it is likely that these observations will be similar for all HPRTs. Because the chemical step is not rate limiting for these enzymes, the observed k_{cat} from steady-state kinetics does not reflect solely the rate for the chemistry of the reaction but instead is influenced by the rate of product release.

Truncation of the Asp137 side chain to alanine resulted in a 30-fold reduction in catalytic efficiency, arising almost entirely from a reduction in k_{cat}. Surprisingly, the isosteric replacement in the D137N mutant was more deleterious, causing a 40-fold reduction in k_{cat}/K_m as compared to WT.

Table 3: Kinetic Parameters for the Forward Reaction Catalyzed by the Wild-Type and Mutant HPRTs

	hypoxanthine (pH 7.5)[a]			hypoxanthine (pH 9.6)[b]			PRPP (pH 7.5)		
	k_{cat} (s^{-1})	K_m (μM)	k_{cat}/K_m ($s^{-1}\,\mu M^{-1}$)	k_{cat} (s^{-1})	K_m (μM)	k_{cat}/K_m ($s^{-1}\,\mu M^{-1}$)	k_{cat} (s^{-1})	K_m (μM)	k_{cat}/K_m ($s^{-1}\,\mu M^{-1}$)
WT	18	8.6 ± 1.5	2.1	19	28 ± 3.2	0.69	22	35 ± 2.9	0.61
D137E	10	14 ± 2.0	0.70	12	27 ± 3.8	0.46	6.7	6.7 ± 1.1	1.0
D137Q	3.2	15 ± 1.2	0.22	4.7[c]	140	0.03	4.1	21 ± 2.0	0.20
D137N	1.6	31 ± 4.1	0.05	4.1	39 ± 5.8	0.01	2.5	11 ± 1.4	0.24
D137A	0.60	8.3 ± 1.9	0.07	2.1	27 ± 4.1	0.08	0.50	1.6 ± 0.10	0.31

[a] Hypoxanthine exists primarily as the neutral form at pH 7.5. [b] Hypoxanthine exists primarily as the monoanion form at pH 9.6. [c] Limited solubility of hypoxanthine prevented the measurement at saturating concentrations (>200 μM). Therefore, kinetic parameters for the D137Q mutant at pH 9.6 were estimated from double reciprocal plots of the velocity data.

This large reduction in activity was not caused by the chemical nature of the carboxamide side chain because the longer carboxamide of D137Q resulted in catalytic efficiency that was only 10-fold below that for WT. The D137E mutant was most similar to WT with only a 3-fold reduction in k_{cat}/K_m. Although the isosteric aspartate to asparagine replacement resulted in a dramatic reduction in enzyme activity, the activities of the isosteric glutamate and glutamine mutants were surprisingly similar (within 3-fold).

The K_m's for hypoxanthine for most of the mutants were within 2-fold of WT, while the D137N mutant displayed the greatest effect with a K_m 4-fold higher than WT. When the pH of the assay buffer was raised to 9.6, a dramatic increase in the K_m for hypoxanthine was observed for the D137Q mutant, while the other mutants had K_m's similar to WT. In addition, notably elevated k_{cat}'s were observed for the D137N and D137A mutants at pH 9.6 relative to pH 7.5. In contrast to the activities observed with varying hypoxanthine concentrations, the catalytic efficiencies of the mutants with varying PRPP concentrations were all within 3-fold of WT, primarily due to decreases in the K_m's for PRPP of the mutants relative to WT that compensate for their lower k_{cat}'s.

pH−Activity Studies. The effect of pH on activity for WT and mutant enzymes (D137E, D137Q, D137N, D137G, D137V, and D137A) enable direct comparisons of the ionic states of the side chains and the chemical requirement at this position for effective enzyme catalysis. The dependence of the reaction rate on pH (pH−rate profile) was measured at saturating concentrations of substrates. Therefore, with the exception of the D137Q mutant at higher pH values (discussed below), the profiles reflect the effect of pH on the apparent k_{cat} for the WT and mutant enzymes. The pH−k_{cat} profiles of mutants and the WT enzyme are shown in Figure 1. The pH−k_{cat} profile of the WT enzyme displayed a sigmoidal curve, increasing from pH 4 to 8, then plateauing at higher pH values (Figure 1, panel a). These observations closely resemble the pH−k_{cat} profile previously described for the WT human HPRT (*18*). In contrast, the pH−k_{cat} profile for the D137A mutant lacks the pH-dependence in the acidic limb (Figure 1, panel b) which is observed with the WT enzyme. This result indicates that the ionized carboxylate moiety of Asp137 is the active form required for catalysis. Interestingly, a marked increase in rate at pH values higher than 8 with the D137A mutant was observed and is discussed below. The D137E mutant enzyme displayed a pH−k_{cat} profile similar to the WT enzyme (Figure 1, panel a), further indicating that the ionized carboxylate of Glu137 is the active form in catalysis.

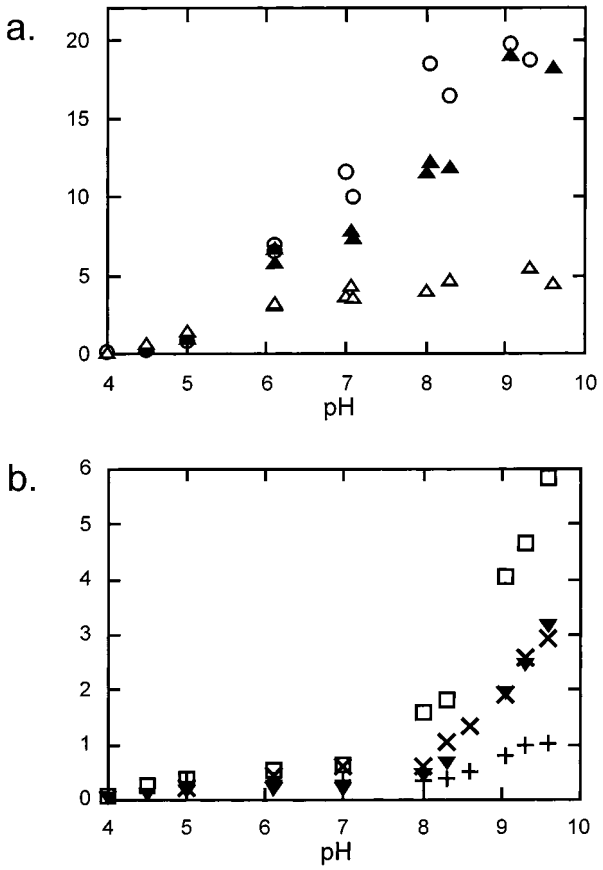

FIGURE 1: The pH−k_{cat} profiles for the forward reaction catalyzed by WT and mutant HPRTs. In panel a are shown the profiles for the wild-type (○), D137E (▲), and D137Q (△) mutant enzymes. In panel b are shown the profiles for the D137G (×), D137N (□), D137A (▼), and D137V (+) mutant HPRTs.

The D137Q mutant exhibited only a slight response of k_{cat} to pH as compared to the D137E and WT enzymes (Figure 1, panel a). The k_{cat} for D137Q increases slightly between pH 4 and pH 7.0 but fails to increase further above pH 7. For this mutant, at pH values above 7, the concentration of hypoxanthine required to achieve saturation exceeded the solubility limit of 400 μM in the assay. Thus, the rates for the D137Q mutant at higher pH values no longer represent the k_{cat} for the enzyme. Steady-state kinetic analysis demonstrated that the K_m for hypoxanthine is markedly increased at pH 9.6 (Table 3). This dramatic change in K_m at pH 9.6 was not observed for the other mutant enzymes nor for WT. Ionization of the Gln137 side chain is unlikely (the pK_a of formamide is 17.2) (*40*, *41*). Thus, the increase in the rate of the D137Q between pH 4 and pH 7.0 does not

reflect the ionization of the side chain but alternatively could reflect the involvement of water molecules in the positioning and function of the glutamine side chain.

Mutants with relatively low activities (D137G, D137N, and D137V) shared similar pH−rate profiles with the D137A mutant (Figure 1, panel b). These profiles lack the pH dependence over the range of pH 4−7.5 and displayed increasing reaction rates at pH values above 8. Although the side chain of asparagine has the same functional group as glutamine, the D137N mutant has very low activity and yields a pH−k_{cat} profile similar to that for D137A (Figure 1, panel b), strongly suggesting that, unlike Gln137, the side chain of Asn137 does not participate in catalysis. A similar pH profile was reported for the D137N mutant of the human HPRT (*18*). Although D137A, D137G, D137N, and D137V enzymes are relatively inactive, the shared increase in rates for these mutants at pH values above 8 is intriguing. None of these mutants possess an ionizable side chain at position 137. The similarity of the pH−rate profiles for these mutant enzymes suggest that they share a common mechanism, while the differences in the chemical nature of the amino acid substitutions indicate that the observed increase in rate may reflect the ionization of the substrate rather than the enzyme.

Substrate Ionization. The reported pK_a values for PRPP are 5.9 and 6.7 (*42*). Previous kinetic (*31*, *43*) and structural (*11*) studies showed that a coordination complex of PRPP and two magnesium ions is the substrate for the reaction catalyzed by HPRTs. This complex is estimated to have pK_a values closer to 4 and 4.7 (*44*−*46*). Therefore, the observed increase in the catalytic rates of these mutants at pH > 8 probably does not reflect change in the reactivity of PRPP upon ionization. On the other hand, hypoxanthine has three pK_a values: 2.3, 8.4, and 12.4, which reflect the existence of monocation, monoanion, and dianion forms, respectively (*47*). Neutral hypoxanthine is ionized to the monoanion form at pH > 8.4, roughly paralleling the observed increases in activities for the mutants with low activities. These results are consistent with increasing nucleophilicity of the monoanion form of hypoxanthine. Steady-state kinetic studies at pH 9.6 (Table 3) indicated that the monoanion form of hypoxanthine can bind the HPRTs and be used as a substrate, confirming a previous report which suggested that the HPRT utilized the ionized hypoxanthine at alkaline pH (*48*). Relative to pH 7.5, at pH 9.6 there are only slight increases in the K_m values for hypoxanthine with the WT and most of the mutant enzymes (Table 3). In contrast, the D137Q mutant displayed a large decrease in the overall catalytic efficiency (k_{cat}/K_m) at the higher pH value due almost entirely to a 10-fold increase in the K_m for hypoxanthine (Table 3).

Crystal Structures of D137 Mutants. Crystal structures of four of the mutants (A, E, Q, and N) were determined and refined at moderately high resolution (1.72 to 2.06 Å) (Table 4). The crystallization strategy previously used for the WT enzyme (*11*), using as ligands the substrate PRPP and a hypoxanthine analogue HPP, was again used here to capture structures of the ternary substrates complexes of the mutant proteins. With the WT and mutant enzymes, this crystal form results in a dimeric structure that reveals two independent views of the substrates-bound active site, with the long flexible loop (loop II) of one subunit in an open conformation and in the other subunit in a closed conformation. The overall crystal structure of the D137A mutant was superimposable (0.29 Å rmsd on Cα positons) with the WT enzyme (*11*). No other side chains occupied the void left by the alanine substitution at position 137. The only significant differences between the two structures were the lack of the aspartic acid side chain and shifts in positions for some of the crystallographic water molecules (Figure 2). For the other three mutants, the rmsd's with the WT structure on Cα positions were 0.16 Å for D137E, 0.17 Å for D137Q, and 0.28 Å for D137N, respectively. The structures of the mutant enzymes provide detailed views of the interactions between substrate ligands and the side chains at position 137 and help to clarify the interpretation of the functional analyses with the mutant HPRTs.

Table 4: Crystallographic Summary

	D137A	D137E	D137N	D137Q
Diffraction Data				
space group	$P2_1$	$P2_1$	$P2_1$	$P2_1$
a (Å)	39.4	39.5	39.6	39.4
b (Å)	102.2	101.9	103.5	101.3
c (Å)	52.0	51.8	52.1	51.7
β (deg)	94.1	94.2	93.9	94.2
resol range (Å)	30.0−1.84	40.0−1.92	20.0−1.72	30.0−2.06
(high-res bin)	(1.89−1.84)	(1.96−1.92)	(1.76−1.72)	(2.11−2.06)
unique refl (no.)	33269	29078	44365	21963
complete (%)[a]	95.8	96.4	99.9	92.1
	(93.7)	(89.5)	(99.5)	(56.2)
R_{sym}[b]	0.056	0.065	0.061	0.068
	(0.400)	(0.377)	(0.272)	(0.411)
$\langle I/\sigma(I)\rangle$	13.7	17.8	31.3	17.3
	(2.9)	(3.2)	(3.2)	(2.6)
redundancy	2.3	3.9	4.8	4.5
source[d]	NSLS × 12B	SSRL 7−1	APS 5IDB	UNCryst
Refinement				
resol range (Å)	6.0−1.84	6.0−1.92	6.0−1.72	6.0−2.06
R_{free}[c]	0.252	0.241	0.267	0.259
R_{cryst}[c]	0.192	0.177	0.210	0.168
protein atoms	2995	3028	2991	3028
ligand atoms	81	78	78	78
solvent atoms	178	230	158	199
average B-factor (Å^2)				
protein	20.2	20.6	25.7	20.2
ligands open active site	24.6	31.5	25.6	29.6
(closed active site)	(15.6)	(14.4)	(22.6)	(14.7)
solvent	30.9	36.0	38.0	33.2
rmsd from target values				
bond lgth (Å)	0.011	0.010	0.011	0.011
bond ang (deg)	1.57	1.58	1.64	1.62

[a] Completeness is the fraction of theoretically possible reflections observed at least once. [b] $R_{sym} = \sum|I_i - \langle I\rangle|/\sum I_i$, where I_i is the intensity of the *i*th observation and $\langle I\rangle$ is the mean intensity of the reflection. [c] $R_{cryst} = \sum|F_o - F_c|/\sum|F_o|$. R_{free} a 5−8% subset of the reflections from each dataset were used for this calculation. [d] NSLS, National Synchrotron Light Source; SSRL, Stanford Synchrotron Radiation Laboratory; APS, Advanced Photon Source, 5IDB is a beamline of the Dupont-Northwestern-Dow collaborative access team (DND-CAT) at Argonne National Lab; UNCryst, University of North Carolina at Chapel Hill.

Correlation of Functional and Structural Observations. The availability of steady-state kinetic analyses, pH−k_{cat} profiles, and crystal structures for the four mutant enzymes and WT provide a unique opportunity for detailed structure/function analysis of the role of Asp137 in catalysis by HPRTs. The results of the functional studies were validated and/or clarified using the molecular details revealed in the crystal structures, as discussed for each mutant enzyme below.

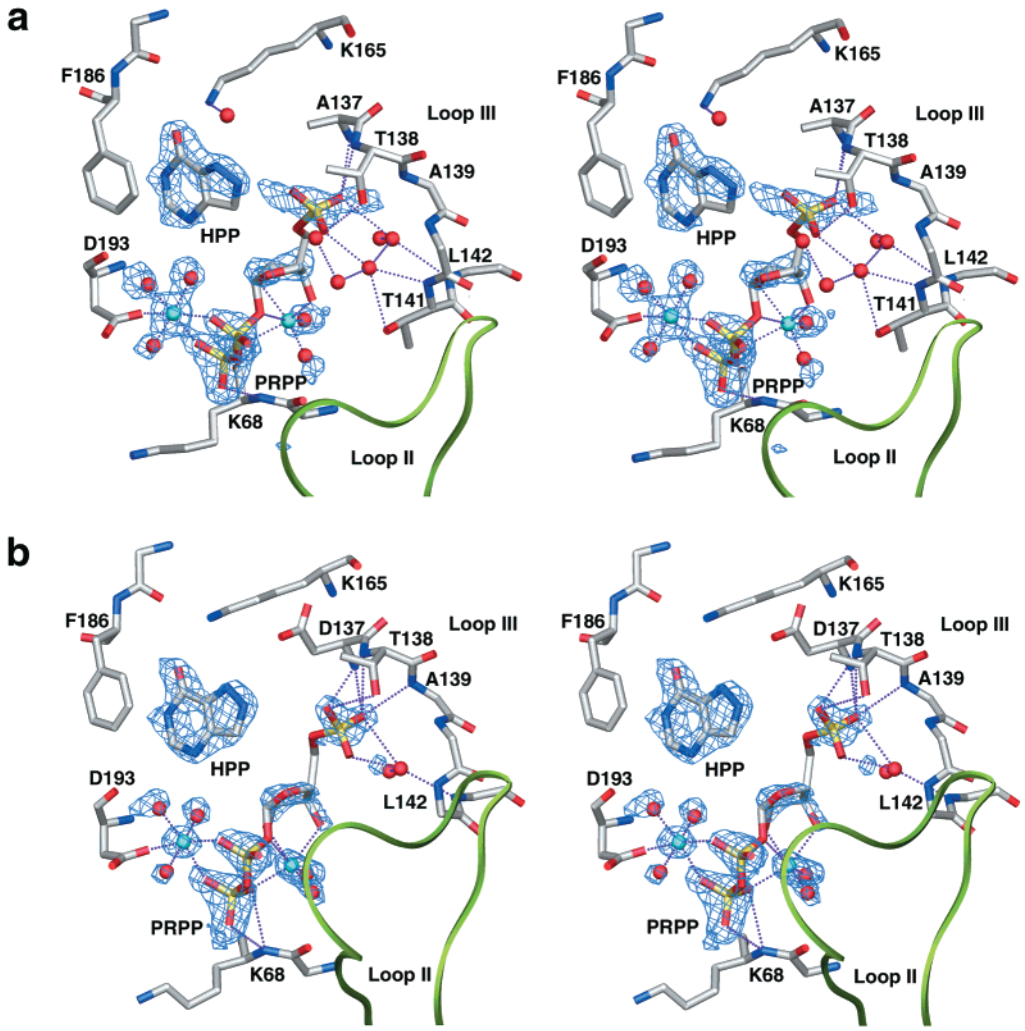

FIGURE 2: The structures of the open active sites of the D137A mutant and WT HPRTs. Panels a and b are stereoviews of the active sites in the open subunits of the D137A mutant and WT HPRT, respectively. The main chain of the flexible loop (loop II) is displayed as a green ribbon. Atoms are shown in standard colors, with octahedrally coordinated magnesium ions shown in cyan, their coordinaing waters and other crystallographic waters illustrated by red spheres. Dotted lines represent interatomic distances ≤3.2 Å. The $|F_o - F_c|$ omit electron density maps of bound ligands are contoured at 3.0σ.

The D137A Mutant. Deletion of the carboxylate side chain at position 137 by alanine substitution (D137A) reduced the k_{cat} by 30-fold (Table 3), suggesting that Asp137 participates in catalysis. Although the K_m for hypoxanthine was largely unaffected, there was a 22-fold decrease in the K_m for PRPP in the D137A mutant. This reduction in the K_m for PRPP is consistent with studies of a D137A mutant of HPRT from *Toxoplasma gondii* (*15*). The absence of a proximal charge repulsion between the carboxylate side chain of Asp137 and the 5-phosphate group of PRPP in the active site could contribute to the large decrease in the K_m for PRPP. In the mutant enzyme, PRPP apparently binds with high affinity but in a conformation that is nonproductive for catalysis; whereas, in the wild-type enzyme, the charge repulsion between the Asp137 and the 5-phosphate weakens binding interactions but results in enzyme−substrate interactions that are more productive for catalysis. This hypothesis is supported by the crystal structure of the D137A mutant enzyme (Figure 2).

Electron density for the 5-phosphate of PRPP in the open subunit of the D137A enzyme is not well-defined and suggests that the phosphate moiety is not well-anchored in its binding loop (loop III) and may assume more than one conformation (Figure 2, panel a). The temperature factors of protein atoms surrounding the 5-phosphate in the open subunit of D137A are uniform and range from 10 to 15 Å^2, while the temperature factors for the 5-phosphate group itself are 20−25 Å^2 higher, ranging from 35 to 45 Å^2 indicating its increased mobility. Three additional well-ordered water molecules are accommodated in the space below the 5-phosphate group of PRPP in the D137A structure and have temperature factors of 14−24 Å^2. By contrast, density for the 5-phosphate group of PRPP defines a single position in the WT active site, well anchored by a series of hydrogen bonds primarily to the main chain of loop III (*11*). In the WT enzyme, the carboxylate of Asp137 may repel the 5-phosphate moiety such that it is stable only when positioned deep inside the loop III binding pocket, remote from the aspartate at 137. This proposed repulsion is consistent with the observed decrease in K_m for PRPP in the D137A mutant in which the repulsion would be absent. The electrostatic repulsion exerted by Asp137 might be weakened as the carboxylate side chain and the 5-phosphate of PRPP form hydrogen bonds with the hydroxyl group of Tyr104 as the flexible loop II closes over the active site just prior to the catalytic step. These interactions are observed in crystal

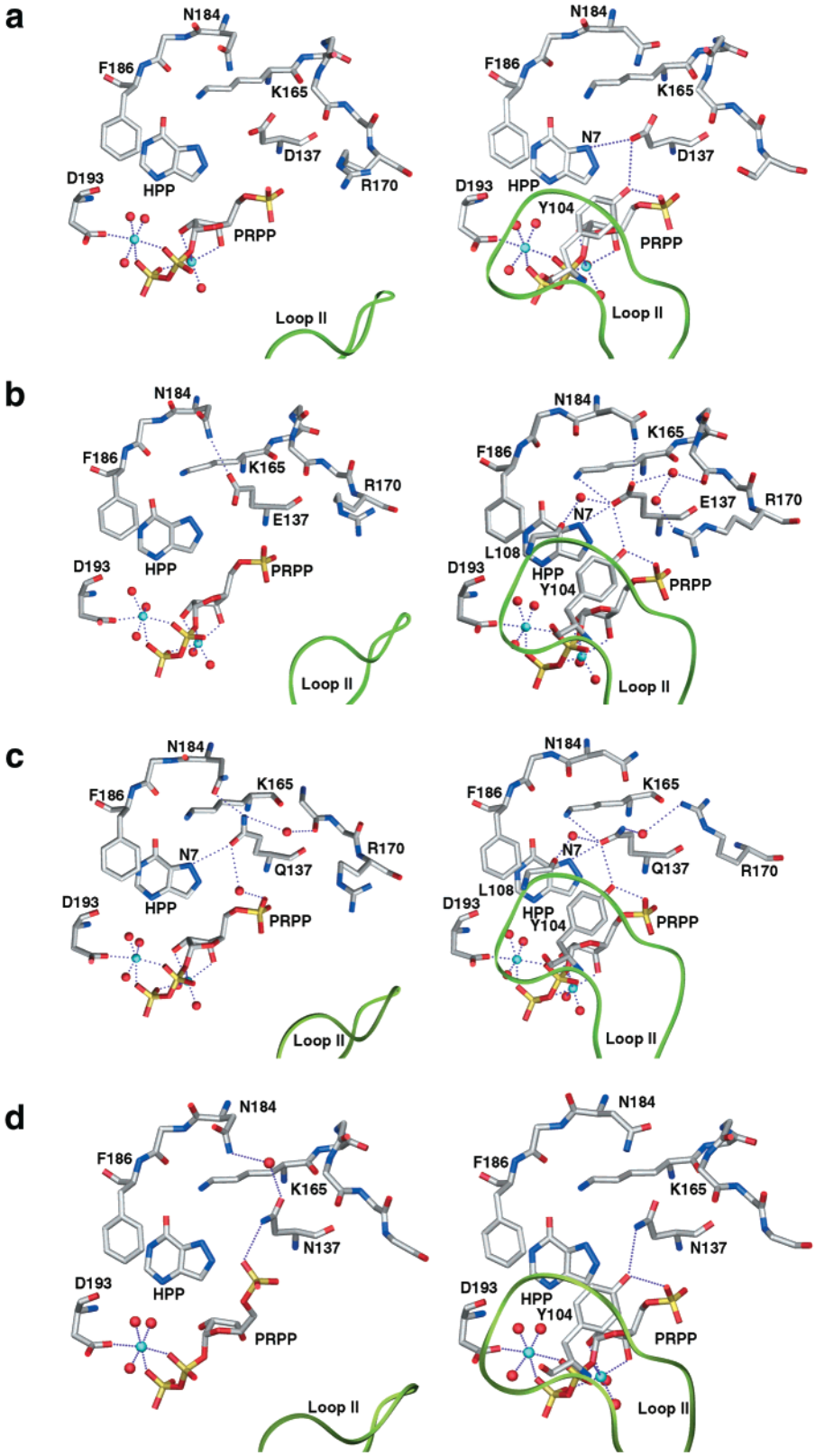

FIGURE 3: Structures of the open and closed active sites in various mutant forms of the trypanosomal HPRT. Active sites of open and closed subunits are shown on the left and right, respectively. Panel a shows the WT structure (*11*), and panels b, c, and d show the structures of the D137E, D137Q, and D137N mutants, respectively. Dotted lines represent interatomic distances ≤3.5 Å. Atom colors are as described in Figure 2.

structures of the closed subunits of the wild-type and mutant enzymes (Figure 3).

The D137E Mutant. The D137E mutant enzyme displayed a pH−k_{cat} profile similar to the WT enzyme (Figure 1, panel a), indicating that the ionized side chain of Glu137 is the active form. In the open subunit of the crystal structure of the D137E mutant, the Glu137 side chain forms a hydrogen bond with the side chain of Asn184 (2.9 Å from Asn184 ND2 to Glu137 OE2). This interaction stabilizes the longer glutamate side chain in a position more remote from the

bound purine analogue than is observed for the aspartate side chain in the open active site of the WT structure (Figure 3, panels a and b). This increased distance could weaken the potential repulsive interaction between the carboxylate side chain of Glu137 and the 5-phosphate of PRPP and could account for the reduced K_m for PRPP exhibited by the D137E mutant as compared to that for WT (Table 3). Therefore, attenuation of enzyme−substrate destabilization in the ground-state could in part contribute to the lower catalytic efficiency of the D137E mutant. Furthermore, the additional methylene group of the Glu137 side chain results in the carboxylate moiety being more exposed to bulk solvent than with Asp137, allowing water molecules to participate in the side chain positioning. In the closed subunit (Figure 3, panel b), the Glu137 side chain is restrained by a unique network of hydrogen bonds. These novel interactions bring the carboxylate side chain into direct contact with HPP, forming a 2.9 Å hydrogen bond (Glu137 OE1 to HPP N7). Thus, the modified microenvironment of the Glu137 side chain could affect its electrostatic force field and consequently reduce its catalytic efficiency as compared to the WT enzyme.

The D137Q Mutant. The D137Q mutant exhibited a unique pH−rate profile with activity increasing slightly from pH 4 to 7 then leveling off at pH values above 7. The lack of a continued increase in activity at higher pH values is likely due to a marked increase of the K_m for the monoanion form of hypoxanthine at pH 9.6 (Table 3). Comparison of open subunits in structures of the WT, the D137E, and the D137Q enzymes (Figure 3, panels a−c) reveals that the carboxylate side chains are more distant from the N7 position of the purine analogue (3.6−4.0 Å) as compared to the glutamine side chain (3.4 Å). Thus, the repulsive interactions with the monanion form of hypoxanthine would be predicted to be severe in the D137Q mutant enzyme, resulting in the increased K_m at pH 9.6. The distance between Gln137 OE1 and HPP N7 shortens nearly 0.7 Å upon loop II closure to favor a strong hydrogen bond between the side chain of Gln137 and HPP (3.4 Å in the open subunit to 2.7 Å in the closed subunit) (Figure 3, panel c). Similar to its structural isostere Glu137, the side chain of Gln137 is more exposed to the bulk solvent and thus permits water molecules to participate in side chain positioning. These water molecules and the Gln137 side chain are well ordered and at full occupancy, with average B-factors of 26.0 and 29.0 Å^2, respectively.

Partial charges on the carboxamide moiety of the Gln137 side chain could be induced by polarization (*49*−*52*). Not only could the hydrogen bond network provided by the water molecules help correctly position the Gln137 side chain for participation in catalysis, but also these interactions could accentuate the polarization of the carboxamide moiety. Stabilization of the polarized resonance form of the carboxamide functional group (*52*) in an appropriate orientation to interact with the purine substrate could further enhance the efficiency of the Gln137 side chain in stabilizing the proposed transition-state by forming a particularly strong hydrogen bond (Figure 4). The k_{cat}/K_m for the D137Q mutant is approximately 3-fold lower than the D137E mutant. This difference in activity may reflect the lower efficiency of a polarized, partial negative charge of the carboxamide side chain in stabilizing the developing partial positive charge on purine N7 in the transition-state, as compared to the

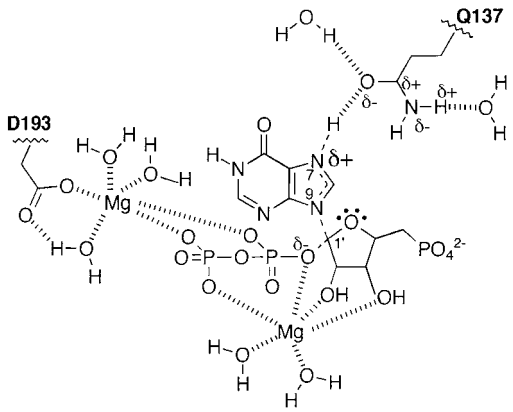

FIGURE 4: Schematic representation of the polarized resonance form of the Gln137 side chain showing hydrogen bond interactions in the proposed transition-state. Broken lines represent hydrogen bond interactions. Dashed lines indicate metal coordination interactions.

efficiency of a fully ionized negative charge achievable by a carboxylate side chain. This observation indicates that a general base at position 137 is not required in the HPRT-catalyzed reaction, as previously suggested (*18*). Instead, the D137Q mutation demonstrates that stabilization of the transition-state by hydrogen bonding is sufficient for catalysis, albeit with 10-fold lower catalytic efficiency.

The D137N Mutant. Although the side chain of Asn137 has the same functional group as Gln137, the D137N mutant has very low activity and yields a similar pH−rate profile as D137A and other mutants with low activity (Figure 1, panel b). In fact, the overall catalytic efficiency of D137N with hypoxanthine is lower than that for D137A (40- versus 30-fold less than wild-type, respectively). These results strongly suggest that the side chain of Asn137 does not participate in catalysis. An explanation is provided by the crystal structure of the D137N mutant. In this structure, the carboxamide side chain of Asn137 assumes a distinct rotamer from that of Gln137 (Figure 3, panels c and d). The short distance between the carboxamide side chain and the 5-phosphate of PRPP in the open subunit of the D137N mutant reveals that this rotamer participates in a strong hydrogen bond between the Asn ND2 and PRPP O3P (2.75 Å). This attractive interaction alters the position and interactions available to the 5-phosphate of PRPP in the open subunit of D137N mutant, as compared to the WT enzyme (Figure 5). In the open active site, the asparagine side chain is further stabilized in this conformation by a hydrogen bond formed between an active site water molecule which is also bound to Asn184. Therefore, the Asn137 side chain is locked in a nonfunctional rotamer (Figure 3, panel d). In addition, a shift in the position the 5-phosphate of PRPP causes a steric clash with the purine substrate (2.6 Å between HPP N8 and PRPP O3P) and likely contributes to the large increase in the K_m for hypoxanthine observed for this mutant.

In the closed subunit, the distance between the Asn137 ND2 and HPP N7 is about 3.9 Å, consistent with a failure to form a hydrogen bond between the asparagine side chain and the bound HPP. These results clarify the difference in functional consequences between D137N and D137Q mutants. The asparagine substitution does not represent a simple isosteric replacement of a carboxamide moiety for the carboxylic acid moiety of aspartate. Instead, the D137N crystal structure reveals unanticipated novel interactions that

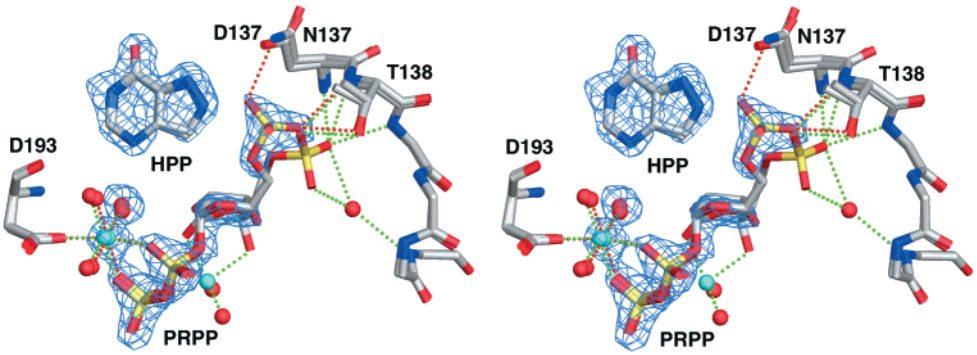

FIGURE 5: Comparison of open subunits of the D137N mutant and WT HPRTs. Stereoview of the $|F_o - F_c|$ omit maps for the bound PRPP and HPP in the D137N mutant are shown in cyan contoured at 3.8σ, overlayed on the superimposed D137N and WT crystal structures. Hydrogen bonds between the 5-phosphate of PRPP with the enzyme are shown in red (for D137N) and green (for WT) dotted lines. Atom colors are as described in Figure 2.

prevent the shorter carboxamide of asparagine from interacting with the purine ligand in a manner similar to either the aspartate of WT or the glutamine mutant. In contrast, comparisons of the glutamine (D137Q) with the gluatamate (D137E) mutant does provide a valid test of the replacement of a carboxamide for a carboxylate functional group at 137. The catalytic efficiency of D137Q is only 3-fold lower than that for D137E and their structures are very similar, thus showing that a carboxamide side chain is capable of participating in catalysis.

Results from previous studies with a D137N mutant of the human HPRT (*18*) suggested that Asp137 acts as a general base, as previously proposed from structural data (*6*). The positions of the invariant Asp137 and bound ligands are conserved among several crystal structures of 6-oxopurine phosphoribosyltransferases despite a wide diversity of pH values and precipitants used in the crystal growth conditions (*6*, *8*, *11*−*16*). Therefore, the asparagine substitution in the human HPRT (D137N) would be expected to cause similar structural changes to those observed in the structure of the trypanosomal D137N mutant presented here. Similar trends for the changes in K_m's for both hypoxanthine (increased K_m) and PRPP (lowered K_m) at neutral pH were observed in the human and trypanosomal D137N mutant HPRTs. In addition, the D137N mutants from both species share similar pH−rate profiles, which resemble that of the trypanosomal D137A mutant. Although the acidic side chains of aspartate and glutamate could function as general bases in catalysis by HPRTs, the present study clearly demonstrates that a mutant with a nonionizable side chain at position 137 (D137Q) is catalytically active. Thus, the residue at position 137 in HPRTs is not required to act as a general base, but instead hydrogen bonding with the N7 of the purine substrate is sufficient for catalysis.

Crystal structures of the human and malarial HPRTs have been determined (*12*, *13*) with bound inhibitor (ImmucillinGP or ImmucillinHP) and magnesium-complexed pyrophosphate, resembling the ternary complexes of enzyme with products (*53*). These structures support a hypothesis that the Asp137 side chain could stabilize an N7-protonated transition-state by hydrogen bonding. A short hydrogen bond (∼2.9 Å) was observed between Asp137 and the protonated nitrogen atom of the inhibitor that is an N7 protonated analogue of IMP. This hydrogen bond could provide transition-state stabilization and contribute to the low K_i reported for this inhibitor (*12*, *13*).

Conclusions. The studies presented here reveal the power of saturation mutagenesis and stringent functional selection to quickly produce and assess the activity of mutant HPRTs to illucidate the functional role of Asp137 in enzyme-catalyzed reactions. The methodology enabled generation of a random library of mutants in a single experiment and avoided bias often introduced by more limited site-directed mutational analysis. The results of biochemical and structural analyses of mutant and WT HPRTs indicate that a general base at position 137 is not absolutely required for activity, but a strong hydrogen bond with the N7 of the purine substrate provides sufficient transition-state stabilization to permit relatively efficient catalysis. This new information about the predicted chemical nature of the transition-state is important for a more complete understanding of the enzyme mechanism, as well as for guiding the structure-based design of inhibitors of the HPRTs from parasites.

ACKNOWLEDGMENT

We are grateful to Aimee Butterworth for technical contributions to this work. Also, we would like to thank Per Nygaard of the University of Copenhagen, Denmark, for contributing the SØ609 strain of *E. coli* and for originally suggesting the bacterial complementation strategy. We thank Duncan Cochran of the University of Queensland, Australia, for providing the *recA* SØ606 strain of *E. coli*, Olivier Frolich of Novartis Products Inc. for providing HPP, and Douglas Freymann of Northwestern University Medical School for use of computer resources during crystallographic refinement and access to the DND-CAT beamline. We also are grateful to Syd Craig, Tom Traut, and Richard Wolfenden for helpful discussions and critical reading of the manuscript. Crystallographic data were measured at three synchrotron beamlines: the Stanford Synchrotron Radiation Laboratory (SSRL) beamline 7-1, the Dupont-Northwestern-Dow Collaborative Access Team (DND-CAT) beamline 5IDB at the Advanced Photon Source (APS) at Argonne National Laboratory, and the National Synchrotron Light Source (NSLS) at Brookhaven National Laboratory, beamline X12B.

REFERENCES

1. Wang, C. C. (1984) *J. Med. Chem. 27*, 1−9.
2. Ullman, B., and Carter, D. (1995) *Infect. Agents Dis. 4*, 29−40.
3. Craig, S. P., III, and Eakin, A. E. (1997) *Parasitol. Today 13*, 238−241.

4. Freymann, D. M., Wenck, M. A., Engel, J. C., Feng, J., Focia, P. J., Eakin, A. E., and Craig, S. P., III. (2000) *Chem. Biol. 7*, 957−968.
5. Scully, D. G., Dawson, P. A., Emmerson, B. T., and Gordon, R. B. (1992) *Hum. Genet. 90*, 195−207.
6. Eads, J. C., Scapin, G., Xu, Y., Grubmeyer, C., and Sacchetteni, J. C. (1994) *Cell 78*, 325−334.
7. Schumacher, M. A., Carter, D., Roos, D. S., and Ullman, B. (1996) *Nat. Struct. Biol. 3*, 881−887.
8. Somoza, J. R., Chin, M. R., Focia, P. J., Wang, C. C., and Fletterick, R. J. (1996) *Biochemistry 35*, 7032−7040.
9. Xu, Y., Eads, J., Sacchettini, J. C., and Grubmeyer, C. (1997) *Biochemistry 36*, 3700−3712.
10. Focia, P. J., Craig, S. P., III., Nieves-Alicea, R., Fletterick, R. J., and Eakin, A. E. (1998) *Biochemistry 37*, 15066−15075.
11. Focia, P. J., Craig, S. P., III, and Eakin, A. E. (1998) *Biochemistry 37*, 17120−17127.
12. Shi, W., Li, C. M., Tyler, P. C., Furneaux, R. H., Cahill, S. H., Girvin, M. E., Grubmeyer, C., Schramm, V. L., and Almo, S. C. (1999) *Biochemistry 38*, 9872−9880.
13. Shi, W., Li, C. M., Tyler, P. C., Furneaux, R. H., Grubmeyer, C., Schramm, V. L., and Almo, S. C. (1999) *Nat. Struct. Biol. 6*, 588−593.
14. Héroux, A., Lucile White, E., Ross, L. J., and Borhani, D. W. (1999) *Biochemistry 38*, 14485−14494.
15. Héroux, A., Lucile White, E., Ross, L. J., Davis, R. L., and Borhani, D. W. (1999) *Biochemistry 38*, 14495−14506.
16. Craig, S. P., III, and Eakin, A. E. (2000) *J. Biol. Chem. 275*, 20231−20234.
17. Vos, S., Parry, R. J., Burns, M. R., de Jersey, J., and Martin, J. L. (1998) *J. Mol. Biol. 282*, 875−889.
18. Xu, Y., and Grubmeyer, C. (1998) *Biochemistry 37*, 4114−4124.
19. Schultz, S. C., and Richards, J. H. (1986) *Proc. Natl. Acad. Sci. U.S.A. 83*, 1588−1592.
20. Climie, S., Ruiz-Perez, L., Gonzales-Pacanowska, D., Prapanwattana, P., Cho, S., Stroud, R., and Santi, D. V. (1990) *J. Biol. Chem. 265*, 18776−18779.
21. Canyuk, B., Craig, S. P., III, and Eakin, A. E. (1998) *Appl. Microbiol. Biotechnol. 50*, 181−186.
22. Jochimsen, B. J., Nygaard, P., and Vestergaard, T. (1975) *Mol. Gen. Genet. 143*, 85−91.
23. Craig, S. P., III, Yuan, L., Kuntz, D. A., McKerrow, J. H., and Wang, C. C. (1991) *Proc. Natl. Acad. Sci. U.S.A. 88*, 2500−2504.
24. Eakin, A. E., Guerra, A., Focia, P. J., Torres-Martinez, J., and Craig, S. P., III. (1997) *Antimicrob. Agents Chemother. 41*, 1686−1692.
25. Ho, S. N., Hunt, H. D., Horton, R. M., Pullen, J. K., and Pease, L. R. (1989) *Gene 77*, 51−59.
26. Sambrook, J., Fritsch, E. F., and Maniatis, T. (1989) *Molecular Cloning: A Laboratory Manual*, 2nd ed., Cold Spring Harbor Laboratory, New York.
27. Young, A., and Blakesley, R. (1991) *Focus (BRL) 13*, 137.
28. Fan, J., Ranu, R. S., Ruan, C., and Fuller, C. W. (1996) *BioTechniques 21*, 1132−1137.
29. Yuan, L., Craig, S. P., III, McKerrow, J. H., and Wang, C. C. (1990) *J. Biol. Chem. 265*, 13528−13532.
30. Lee, C. C., Craig, S. P., III, Eakin, A. E. (1998) *Biochemistry 37*, 3491−3498.
31. Yuan, L., Craig, S. P., III, McKerrow, J. H., and Wang, C. C. (1992) *Biochemistry 31*, 806−810.
32. Otwinowski, Z. (1993) *Oscillation Data Reduction Program*, SERC Daresbury Laboratory, Warrington.
33. Brünger, A. T. (1992) *Nature 355*, 472−475.
34. Brünger, A. T. (1992) *XPLOR Version 3.1. A System for X-ray Crystallography and NMR*, Yale University Press, New Haven, CT.
35. Jones, T. A., Zou, J. Y., Cowan, S. W., and Kjeldgaard, M. (1991*) Acta Crystallogr. A47*, 110−119.
36. Evans, S. V. (1993) *J. Mol. Graph. 11*, 134−138.
37. O'Donohue, M. J., and Kneale, G. G. (1994) *Methods Mol. Biol. 30*, 211−225.
38. Airaksinen, A., and Hovi, T. (1998) *Nucleic Acids Res. 26*, 576−581.
39. Wanner, B. L. (1987) in *Escherichia coli and Salmonella typhimurium: Cellular and Molecular Biology* (Neidhardt, F. C., Ingraham, J. L., Low, K. B., Magasanik, B., Schaechter, M., and Umbarger, H. E., Eds.) pp 1326−1333, American Society for Microbiology, Washington, DC.
40. Homer, R. B., and Johnson, C. D. (1970) in *The Chemistry of Amides* (Zabicky, J., Ed.) pp 187−243, Wiley, New York.
41. Perrin, C. L. (1994) *Science 266*, 1665−1668.
42. Dawson, R. M. C., Elliott, D. C., Elliott, W. H., and Jones, K. M. (1986) *Data for Biochemical Research*, 3rd ed., Clarendon, Oxford.
43. Salerno, C., and Giacomello, A. (1981) *J. Biol. Chem. 266*, 3671−3673.
44. Smith, R. M., and Alberty, R. A. (1955) *J. Am. Chem. Soc. 78*, 2376−2380.
45. Smith, R. M., and Alberty, R. A. (1955) *J. Phys. Chem. 60*, 180−184.
46. Phillips, R., Eisenberg, P., George, P., and Rutman, R. J. (1965) *J. Biol. Chem. 240*, 4393−4397.
47. Lichtenberg, D., Bergmann, F., and Neimal, Z. (1972) *Isr. J. Chem. 10*, 805−817.
48. Olsen, A., and Milman, G. (1974) *J. Biol. Chem. 249*, 4030−4037.
49. Poland, D., and Scheraga, H. A. (1967) *Biochemistry 6*, 3791−3800.
50. Kitaigorodsky, A. I. (1973) *Molecular Crystals and Molecules*, Academic Press, New York.
51. Maccallum, P. H., Poet, R., and Milner-White, E. J. (1995) *J. Mol. Biol. 248*, 361−373.
52. Milner-White, E. J. (1997) *Protein Sci. 6*, 2477−2482.
53. Smith, J. L. (1999) *Nat. Struct. Biol. 6*, 502−504.

BI001195Q